Available online at www.sciencedirect.com
ScienceDirect
Journal of Power Sources 180 (2008) 354–364
JOURNAL OF POWER SOURCES
www.elsevier.com/locate/jpowsour

Hydrogen production through steam electrolysis: Control strategies for a cathode-supported intermediate temperature solid oxide electrolysis cell

J. Udagawa [a,b], P. Aguiar [b], N.P. Brandon [b,*]

[a] *Imperial Centre for Energy Policy and Technology, Centre for Environmental Policy, Imperial College London, SW7 2AZ, UK*
[b] *Department of Earth Science and Engineering, Imperial College London, SW7 2AZ, UK*

Received 1 October 2007; received in revised form 20 December 2007; accepted 26 January 2008
Available online 8 February 2008

Abstract

Hydrogen production via steam electrolysis may involve less electrical energy consumption than conventional low temperature water electrolysis, reflecting the favourable thermodynamics and kinetics at elevated temperatures. The present paper reports on the development of a one-dimensional dynamic model of a cathode-supported planar intermediate temperature solid oxide electrolysis cell (SOEC) stack with air flow introduced through the cells. The model, which consists of an electrochemical model, two mass balances, and four energy balances, is here employed to study the prospect of the stack temperature control through the variation of the air flow rate. The simulations found that the increase in the air flow rate provides enhanced cooling and heating during exothermic and endothermic operations, respectively. The stack behaviour has suggested that such a convective heat transfer between the cell components and air flow would allow the control of stack temperature. However, only a small dependence of the temperature on the air flow rate was observed for a stack driven at conditions near thermoneutral operation, indicating that this operating mode should be avoided from a control perspective.
© 2008 Elsevier B.V. All rights reserved.

Keywords: Hydrogen production; Steam electrolyser; SOEC; Intermediate temperature; Planar; Dynamic model

1. Introduction

Hydrogen is regarded as a leading candidate for alternative future fuels. It has the potential to address the environmental and energy security issues associated with fossil-derived hydrocarbon fuels. Among many hydrogen production methods, water electrolysis is a well-established technique, which is capable of producing carbon-free hydrogen if used in conjunction with renewable or nuclear energy. However, water electrolysis has not had a significant commercial penetration, mainly due to its high electricity consumption and associated high operating cost [1].

Steam electrolysis at elevated temperatures might offer a solution by consuming less electricity than is required at ambient conditions through favourable thermodynamics and kinetics [2]. Such a method of hydrogen production is performed using a solid oxide electrolysis cell (SOEC), which can be seen in simple terms as the reverse operation of a solid oxide fuel cell (SOFC), allowing the opportunity to apply recent developments in SOFCs to the field. An SOEC consists of a three-layer solid structure (composed of porous cathode, electrolyte and porous anode) and an interconnect plate. Steam is introduced at the cathode side of the solid structure where it is reduced to hydrogen, releasing oxide ions in the process. The oxide ions then migrate through the electrolyte to the anode where they combine to form oxygen molecules, releasing electrons. Although the use of proton conductors has also been investigated [3–5], yttria-stabilised zirconia (YSZ), which is an oxide ion conductor, is generally used for the electrolyte in SOECs. Typical materials for the cathode are nickel-YSZ cermets and those for the anode are perovskite oxides such as lanthanum manganite.

In SOFC technologies, there is increased interest in intermediate temperature SOFCs (IT-SOFCs), which typically operate between 823 and 1073 K, to allow for a wider range of materials, more cost effective SOFC fabrication methods [6] and increased durability. The reduction in operating temperature has also been seen in the field of SOECs in the limited number of experimental projects reported over recent decades [7–9], where the

* Corresponding author. Tel.: +44 20 7594 5704; fax: +44 20 7594 7444.
E-mail address: n.brandon@imperial.ac.uk (N.P. Brandon).

0378-7753/$ – see front matter © 2008 Elsevier B.V. All rights reserved.
doi:10.1016/j.jpowsour.2008.01.069

Nomenclature

C_i	concentration of gas species i in the anode gas streams (mol m^{-3})
C_{O_2}, C_{N_2}	concentration of oxygen and nitrogen in the anode gas streams (mol m^{-3})
C_i^0	concentration of gas species i at the stack inlet (mol m^{-3})
$C_{O_2}^{TPB}$	concentration of oxygen at the triple phase boundary (mol m^{-3})
$D_{eff,\ anode}$	average effective diffusivity coefficient of the anode (m^2 s^{-1})
f_A^0	inlet flow rate of the anode streams (mol s^{-1})
F	Faraday's constant (C mol^{-1})
h_A	height of the anode gas channels (m)
j	local current density (A m^{-2})
$\bar{j}$	average current density (A m^{-2})
$j_{0,\ anode}$	exchange current density of the anode (A m^{-2})
L	cell length (m)
R	reaction rate (mol s^{-1} m^{-2})
$\Re$	gas constant (J mol^{-1} K^{-1})
t	time (s)
T_A, T_S	temperature of the anode gas streams and solid structure (K)
u_A	velocity of the anode gas streams (m s^{-1})
W	cell width (m)
x	axial coordinate (m)
$y_{O_2}^{mole}$	mole fraction of oxygen in the anode gas streams

Greek letters

α	transfer coefficient
$\eta_{act,\ anode}$	activation overpotential losses at the anode (V)
$\eta_{conc,\ anode}$	concentration overpotential losses at the anode (V)
ν_i	stoichiometric coefficient of gas species i
ν_{O_2}	stoichiometric coefficient of oxygen
τ_{anode}	thickness of the anode (m)
ψ	air ratio

temperature at which the cells are tested has decreased from 1273 to 1073 K. Initially SOECs were developed as tubular cell structures to avoid sealing problems, which is a major issue in segregating the produced H_2 and O_2 in planar cells, particularly over multiple thermal cycles [10]. Today, despite such sealing difficulties, the trend in cell design is to employ planar structures. A planar structure permits high packing density and significantly smaller hot volume in the system than that allowed by a tubular design [11], together with lower manufacturing costs and shorter current paths, reducing the ohmic cell resistance [12]. A planar SOEC can be categorised as being either an electrolyte-supported or electrode-supported design. The former employs the electrolyte as the support structure and is suitable for high temperature operation in which the, often large, ohmic resistance associated with a thick electrolyte can be reduced. In an electrode-supported cell, on the other hand, one of the electrodes

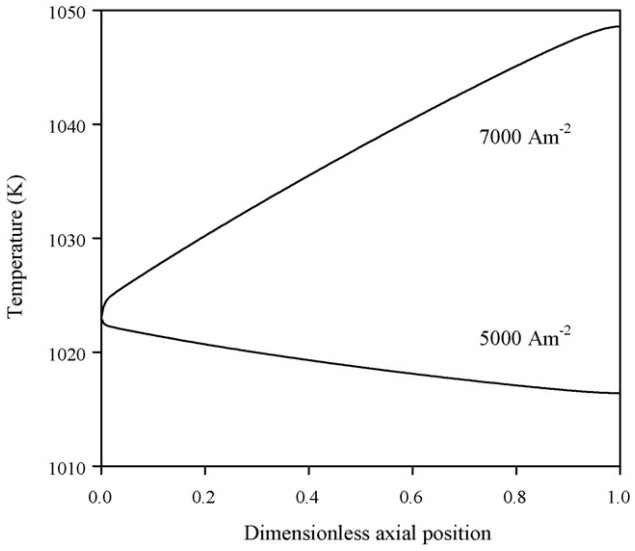

Fig. 1. Temperature distribution along the IT-SOEC stack described in a previous publication [13] for average current densities of 7000 and 5000 A m^{-2}, and an inlet temperature of 1023 K.

is the thickest part of the solid structure, supporting a thick film electrolyte typically 10 μm or so in thickness. Such a design has been developed in order to minimise ohmic resistances in SOFCs operating at intermediate temperatures, and may also be applied to intermediate temperature SOECs (IT-SOECs).

To ensure a sufficient rate of H_2 production, an SOEC system must consist of several repeating cells assembled in stacks. An SOEC stack can function in either exothermic, endothermic or thermoneutral operating modes. During the operation of an SOEC system, heat is generated in the stack as the result of irreversible losses due to ohmic resistance and electrode overpotentials. These depend on operating conditions such as the stack temperature and average current density, as well as materials selection and cell and stack geometry. Fig. 1 shows examples of stack temperature distribution, produced by the one-dimensional model of a co-flow IT-SOEC stack described in a previous publication [13]. The modelled stack considers the cells with the flow of H_2 and H_2O on the cathode side, and of pure O_2 on the anode side of the solid structure. As the mixture of H_2 and H_2O travels along the stack (from left to right in the figure), H_2O is consumed by the reaction while H_2 and O_2 are produced. At the inlet to the cathode gas channels, 10 mol% H_2 is assumed sufficient in preventing the oxidation of the electrode material [7], while the inlet to the anode gas channels are sealed to allow the collection of pure O_2 from the outlet. An inlet temperature of 1023 K, an operating pressure of 0.1 MPa and a steam utilisation factor of 80% have been selected. For the steady state simulation with an average current density of 7000 A m^{-2}, the heat generated via irreversible losses exceeds the thermal energy consumed by the endothermic electrolysis reaction. Such a condition is referred to as exothermic stack operation in which the temperature increases along the stack due to the heat accumulation, as indicated by the figure. Although exothermic operation provides the opportunity to bring the inlet gas streams to the operating temperature entirely through the recovery of the heat

from the hotter outlet streams, such an operating mode is characterised by an increased electrical energy consumption by the stack. Conversely, for the simulation with an average current density of 5000 A m^{-2}, the heat generated via irreversible losses is predicted to be smaller than the thermal energy consumed by the reaction. Such a situation corresponds to endothermic stack operation in which the temperature decreases as the reaction proceeds along the stack. Although endothermic operation allows the stack to function with a lower electrical energy consumption, the rate of H_2 production per unit stack area is less than that arising from exothermic operation, evident from the lower average current density. Furthermore, during endothermic operation it is not possible to bring the inlet streams to the operating temperature entirely by heat recovery from the outlet streams. The implication is that an external heat source is required to supply the thermal energy necessary to elevate the inlet stream temperature to the required level. Therefore, in the design of SOEC systems, there is a trade-off between the benefits of partially replacing electrical energy by less expensive thermal energy, against the extra costs involved in engineering the transfer of this thermal energy from external sources. Finally, thermoneutral stack operation occurs when the thermal energy consumed by the reaction is precisely matched by the heat generated via irreversible losses. During this mode of operation, although the outlet streams carry the same amount of thermal energy as the inlet streams, the energy losses associated with the heat recovery process mean that an external heat source and corresponding equipment costs would still be necessary, as in the case of endothermic operation. The electrical energy consumption of the stack during thermoneutral operation is, however, always greater than that during endothermic operation. Therefore, in general, thermoneutral operation is not recommended from an economic perspective [14].

In a previous publication, a one-dimensional distributed dynamic model of a cathode-supported planar IT-SOEC stack has been presented [13]. The steady state simulation of the model predicted an electricity consumption significantly less than that of low temperature stacks commercially available today. However, the dependence of the stack temperature distribution on the average current density, as can be seen in Fig. 1, calls for strict temperature control if such a stack is to be successfully built and used, especially in dynamic operation. Although SOEC systems are often considered for large scale steady state operation in which the input power source may be a nuclear reactor, temperature control becomes essential if the systems are to be used in dynamic operation with intermittent electrical power sources such as wind turbines or photovoltaic cells. To prevent the fracture of delicate stack components during dynamic operation, significant thermal excursions in the stack need to be avoided by the implementation of an effective control strategy. Such a control strategy would also ensure a constant operating mode of the stack, which is an important constraint as the system requirements vary depending on whether the stack is employed in an exothermic, endothermic or thermoneutral mode. One possible solution to achieving the control requirements would be to modify the SOEC design such that one more degree of freedom is available to control the stack temperature. As can be seen in [15], the temperature of SOFC stacks is often controlled by varying the air flow through the cells. Such a strategy may potentially be applied in the case of an SOEC stack where the introduction of air to the anode gas channels would, in addition to controlling the stack temperature, dilute the O_2 by-product. Although this would remove the possibility of generating extra revenues through the sale of pure O_2, it would also reduce the risk of high temperature corrosion, which might otherwise be caused by the exposure of metallic stack and balance of plant components to such a highly oxidising atmosphere at elevated temperatures [16].

Note that the introduction of the air flow to the anode channels would involve extra investment costs for the compressors and heat exchangers as well as the energy costs associated with the operation of such additional system components. These costs would be a function of the operating conditions, system scales as well as the origin of the input energy. In the development of the control strategy, it is important to evaluate such extra costs and their magnitude with respect to the overall cost of the H_2 production as well as to investigate the technical feasibility of the control strategy.

A mathematical model is an important design tool for devices such as an SOEC, which are still in the development stage. It allows the prediction of the behaviour of the device under different process conditions and assists in the optimisation of its performance. In particular, such a model is essential in understanding the response of an electrolyser under steady electrical power input, such as those from the grid or nuclear energy, as well as under an intermittent renewable electrical power input. However, no studies on the control issues or the dynamic response of an SOEC can be found in the literature. The present paper reports on the development of a dynamic model of a conceptual IT-SOEC stack with the air flow introduced through the cells, produced within the gPROMS modelling environment. This paper introduces the IT-SOEC stack model and the results describing the simulated steady state behaviour of such an electrolyser. The prospect of controlling temperature transitions caused by the time dependent demand for hydrogen from the IT-SOEC is discussed. While the developed model has dynamic capability, only the steady state results are analysed here. The dynamic response will be presented in a subsequent publication.

2. IT-SOEC mathematical model

Although the number of modelling activities on electrolysis at elevated temperatures has increased over recent years [13,17–30], the mathematical modelling of SOEC stacks is still not an active research area. Today, only limited modelling studies attempting to describe SOEC stack behaviour can be found [13,25–30] and, to the authors' knowledge, the issue of temperature control within an SOEC stack has not been the focus of any published work. Here, a previously developed dynamic model of a cathode-supported planar IT-SOEC stack [13] has been modified to introduce air flow as a method of controlling stack temperature. Important changes implemented to the previously developed model are described in Sections 2.1–2.4.

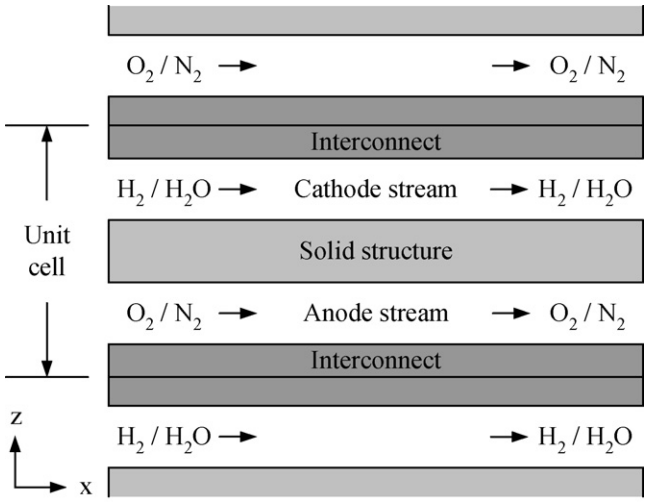

Fig. 2. Schematic view of a planar SOEC stack with the air flow through the anode channels.

In an SOEC system, several repeating cells are assembled in stacks to support a sufficient rate of H_2 production. However, the models of such stacks are usually constructed for the smallest unit cell, which is assumed to describe the response of the whole stack, subject to the use of adequate boundary conditions. Here, the modelled unit cell is considered to be in the centre of a large stack such that end effects can be neglected. Although interconnects normally provide the gas flow channels, above and below the solid structure, the effect of individual passages is neglected. The pressure drop along the gas channels is also assumed to be negligible at the operating pressure of 0.1 MPa, and for the flow rates considered. For the purpose of developing the model, the unit cell is considered to be composed of four components, the cathode and anode gas streams, solid structure and interconnect. Fig. 2 shows the schematic view of such a unit cell with the air flow through the anode gas channel. The model consists of an electrochemical model, mass balances for the cathode and anode streams, and energy balances for the cathode and anode streams, solid structure and interconnect. The properties of the gas streams, solid structure and interconnect are assumed to be constant in order to achieve a more computationally tractable model. This simplification has been assessed in equivalent studies of IT-SOFC stacks in which the stack model employing the constant flow properties, determined at the stack inlet, and that employing the variable flow properties have been compared [31]. The study showed that the simplification is justified provided the average current density is not high. For the IT-SOEC stack model here, to minimise the errors involved in using the constant properties even at relatively high average current densities, the gas properties are averaged over the entire stack length, rather than using those determined at the stack inlet. Finally, ideal gas behaviour is assumed for the cathode and anode streams.

2.1. Anode concentration overpotential losses

Concentration overpotentials occur as mass transport of the gas species involved in the reaction becomes increasingly rate limiting. In the previously developed model, whilst cathode concentration overpotential was included, anode concentration overpotential was not taken into account, on the basis that the difference between the O_2 concentration at the triple phase boundaries TPBs and that in the bulk streams was assumed negligible. However, when air is introduced through the anode channels, such an assumption no longer necessarily applies and it becomes important to include the anode concentration overpotential in the model. Eq. (1) describes the anode concentration overpotential for the IT-SOEC stack with air-fed anode channels. Note that the temperature of the gas mixture at the TPBs is represented by the solid structure temperature. The O_2 concentration at the TPBs is determined for one-dimensional self-diffusion of O_2 in Eq. (2). $D_{\text{eff, anode}}$ represents the average effective diffusivity coefficient in the anode, which is taken as $13.7 \times 10^{-6}\,\text{m}^{-2}\,\text{s}^{-1}$, considering a binary gas mixture of O_2 and N_2 [6]. A method for expressing the mass diffusion activities in an SOFC [32,33] has been adopted for an SOEC in deriving Eq. (2).

$$\eta_{\text{conc,anode}}(x) = \frac{\Re T_S(x)}{4F} \ln\left[\frac{C_{O_2}^{\text{TPB}}(x) T_S(x)}{C_{O_2}(x) T_A(x)}\right] \tag{1}$$

$$C_{O_2}^{\text{TPB}}(x) = C_{O_2}(x) - C_{N_2}(x) - C_{N_2}(x) \times \exp\left[\frac{-j(x)\tau_{\text{anode}}}{4FD_{\text{eff,anode}}[C_{O_2}(x) + C_{N_2}(x)]}\right] \tag{2}$$

2.2. Anode activation overpotential losses

Activation overpotentials are related to the chemical kinetics of the reactions. They are classically determined through the Butler–Volmer equation. In the previously developed model, as the difference between the O_2 concentration at the TPBs and that in the bulk stream was assumed negligible, the simplified form of the Butler–Volmer equation was applied in predicting the anode activation overpotential. Here, the simplified form has been replaced by the extended form (3) to account for the difference in the O_2 concentration created between the TPBs and bulk stream by the introduction of the air flow through the anode channels.

$$j(x) = j_{0,\text{anode}}(x)\left[\exp\left[\frac{2(1-\alpha)F}{\Re T_S(x)}\eta_{\text{act,anode}}(x)\right] - \frac{C_{O_2}^{\text{TPB}}(x)}{C_{O_2}(x)}\exp\left[\frac{-2\alpha F}{\Re T_S(x)}\eta_{\text{act,anode}}(x)\right]\right] \tag{3}$$

2.3. Anode stream mass balance

Although a mass balance can track the changes in the stream compositions, this was not applied to the anode streams in the previously developed model, as the streams of pure O_2 would involve no such changes along the stack. Therefore, for the IT-SOEC stack with air-fed anode channels, an anode stream mass balance must be introduced in the model because the compositions of the anode streams evolve as the mixture of O_2 and

N_2 travels towards the outlet. Here, the anode stream mass balance (4) and the boundary conditions at the inlet (5) predict the O_2 and N_2 concentrations at each location along the stack. The anode stream velocity is assumed constant and determined from the outlet flow rate of the streams.

$$\frac{\partial}{\partial t}[C_i(x)] = -u_A \frac{\partial}{\partial x}[C_i(x)] + \frac{1}{h_A} \nu_i R(x), \quad i \in \{O_2, N_2\} \tag{4}$$

$$C_i(0) = C_i^0, \quad i \in \{O_2, N_2\} \tag{5}$$

2.4. Air ratio

The air ratio reflects the inlet flow rate of air in relation to the rate of reaction. It is here defined as the ratio between the moles of O_2 contained in the inlet air flow to that produced in the unit cell, per unit time. In spite of the slightly different physical definition, the mathematical description of the air ratio, provided in Eq. (6) for an SOEC, is equivalent to that of an SOFC [6]. As will be discussed in the following sections, it would be possible to provide the temperature control for an SOEC stack through the manipulation of the air ratio. Assuming a minimum of 50 mol% N_2 in the anode streams at the stack outlet is required to limit the corrosion of metallic components, the lower bound for the air ratio can be selected to be as small as 0.4. The upper bound is assumed to be 14, namely the maximum air flow rate which can be supplied without incurring significant additional energy costs [15]. Note that for a high air ratio, the anode stream velocity is dominated by the large flow rate of the inlet air. Under such conditions, the increase in the anode stream mass along the stack, which results from the accumulation of the product O_2, has negligible influence over the stream velocity. However as the air ratio is lowered and the flow rate of the inlet air is consequently reduced, such a rising stream mass becomes increasingly more important in accelerating the stream towards the outlet. It is, therefore, important to point out that any inaccuracies incurred in assuming a uniform anode stream velocity in the present model can become progressively larger as the air ratio is reduced.

$$\psi = \frac{2Ff_A^0 y_{O_2}^{mole}}{\bar{j} L W \nu_{O_2}} \tag{6}$$

3. Simulation results and discussion

With the inclusion of Eqs. (1), (2) and (4)–(6) into the previously developed model and the replacement of the simplified Butler–Volmer equation for the anode activation overpotential by the extended form (3), the system of partial differential and algebraic equations for the model of an IT-SOEC stack with air-fed anode channels is solved via the finite difference method using gPROMS Model Builder 3.0.3 [34]. The cathode and anode inlet compositions are assumed to be 10 mol% H_2/90 mol% H_2O and 21 mol% O_2/79 mol% N_2, respectively. The steam utilisation factor is selected to be 80%. The stack geometry and material properties are found in the previous publication. Section 3.1 introduces the steady state performance of the IT-SOEC stack with air-fed anode channels, comparing the reversible potential and irreversible losses to those of the IT-SOEC stack with pure O_2 anode streams. The proposed temperature control strategy through the manipulation of the air ratio is explored in Section 3.2 in which the stack temperature distributions are presented for different values of the air ratio. Section 3.3 discusses the links between such temperature distributions and the local current density along the stack.

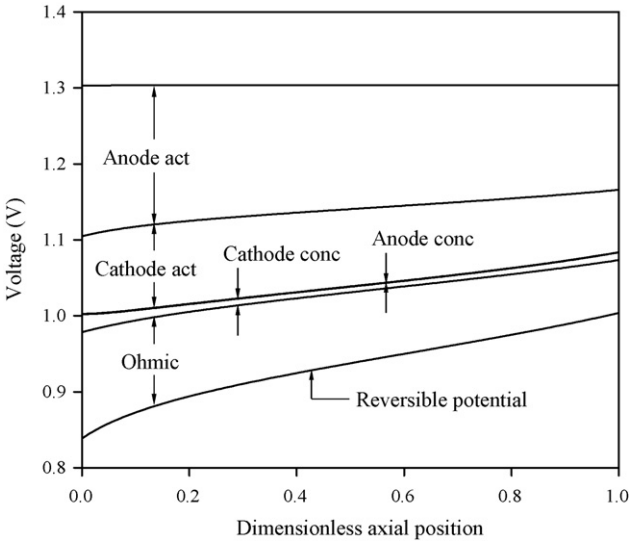

Fig. 3. Reversible potential and irreversible losses along the stack for an average current density of 7000 A m^{-2}, an inlet temperature of 1023 K and an air ratio of 7.

3.1. Steady state performance of IT-SOEC stack with air-fed anode channels

Figs. 3 and 4 present the contributions of the reversible potential and irreversible losses on the cell potential for the IT-SOEC stack with air-fed anode channels at average current densities of 7000 and 5000 A m^{-2}, representing exothermic and endother-

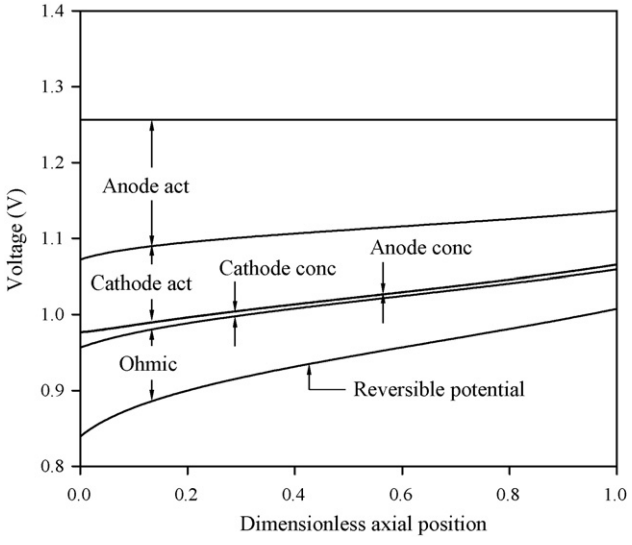

Fig. 4. Reversible potential and irreversible losses along the stack for an average current density of 5000 A m^{-2}, an inlet temperature of 1023 K and an air ratio of 7.

mic operation, respectively. In both cases, the inlet temperature of the anode streams is set equivalent to that of the cathode streams at 1023 K to prevent significant changes in the temperature along the stack near the inlet, and the air ratio has been fixed at 7. Note that, as observed in Fig. 1, the inlet temperature corresponds to the lowest temperature along the exothermic stack and highest temperature along the endothermic stack. The introduction of the air flow at such a temperature, therefore, results in the convective heat transfer between the cell components and air flow, providing cooling and heating to the exothermic and endothermic stacks, respectively. Furthermore, the introduction of the air flow causes a decrease in the O_2 partial pressure in the anode channels, creating the difference between the O_2 concentration at the TPBs and that in the bulk streams. Although this is accounted for in the prediction of the anode concentration overpotential by Eq. (1), both Figs. 3 and 4 indicate that such an irreversible loss is negligible for the conditions employed. As was the case in the IT-SOEC stack with pure O_2 anode streams [13], the activation overpotentials are the predominant source of the irreversible losses.

In Fig. 3, the reversible potential for the exothermic operation of the IT-SOEC stack with air-fed anode channels is predicted to be around 0.027 V lower than that reported in the previous publication for the IT-SOEC stack with pure O_2 anode streams under the same conditions. As illustrated by the Nernst equation, such a reduction in the reversible potential is a consequence of the decrease in the O_2 partial pressure in the anode channels. Although the reduced stack temperature, which results from the convective cooling supplied by the air flow, tends to increase the reversible potential, such an effect is overwhelmed by the influence of the O_2 partial pressure change here. The steady state simulations suggest that the introduction of the air flow, at the air ratio of 7, reduces the average stack temperature from 1038 to 1027 K and the average O_2 partial pressure from 0.10 to 0.02 MPa. By only accounting for the stack temperature change in the Nernst equation, such a temperature reduction alone is expected to increase the average reversible potential by around 0.005 V. On the other hand, the decrease in the average reversible potential which would result only from the effect of the O_2 partial pressure reduction is estimated to be as much as 0.034 V. The impact of the reduced O_2 partial pressure is therefore approximated to be 7 times that of the reduced stack temperature for the conditions employed. However, in spite of the decreased reversible potential, the cell potential shown in Fig. 3 is almost equivalent to that of the IT-SOEC stack with pure O_2 anode streams. This is due to the compensating increase in the ohmic losses and activation overpotentials, of around 0.034 V on average along the stack, caused by the fall in the stack temperature.

Similarly to Fig. 3, Fig. 4 shows the reversible potential for the IT-SOEC stack with air-fed anode channels to be lower than that reported in the previous publication for the IT-SOEC stack with pure O_2 anode streams during endothermic operation. However, noticeable differences in the irreversible losses are not observed here because the temperature of the endothermic stack has not been altered significantly by the introduction of the air flow. As will be explained in Section 3.2, the reduction in the O_2 partial pressure, associated with the dilution of the anode streams by the air flow, increases the thermal energy consumed by the electrolysis reaction per mole of product H_2. Such an increased thermal energy consumption results in the increased amount of heat removed from the stack and has an effect of decreasing the stack temperature. Although this effect complements the convective cooling supplied by the air flow during exothermic operation, it competes against the convective heating during endothermic operation. Therefore, the temperature of the endothermic stack is not altered to the same extent as that of the exothermic stack by the introduction of the air flow.

3.2. Stack temperature control through air ratio manipulation

The temperature distribution along the IT-SOEC stack with air-fed anode channels operated at average current densities of 7000 and 5000 A m^{-2} are respectively illustrated in Figs. 5 and 6. The air ratio is varied between 0.4 and 14 while the inlet temperature is maintained at 1023 K. As can be seen from both figures, the increase in the air ratio causes the stack temperature to become more uniformly distributed, approaching the temperature of the inlet streams. Such a stack behaviour suggests that the increase in the air ratio provides enhanced cooling for the stack during exothermic operation, and enhanced heating during endothermic operation, via the increase in the convective heat transfer between the cell components and air flow. As detailed previously [13], an increase in average current density causes the irreversible losses to increase. During exothermic operation, the consequent rise in stack temperature may be counteracted by increasing the air ratio. Conversely, if the average current density is reduced during exothermic operation, the fall in stack temperature may be avoided by decreasing the air ratio. During endothermic operation, on the other hand, the rise in the stack temperature associated with the increased average current density may be balanced by a decrease in the air ratio, and the fall in the stack temperature corresponding to a reduction in the

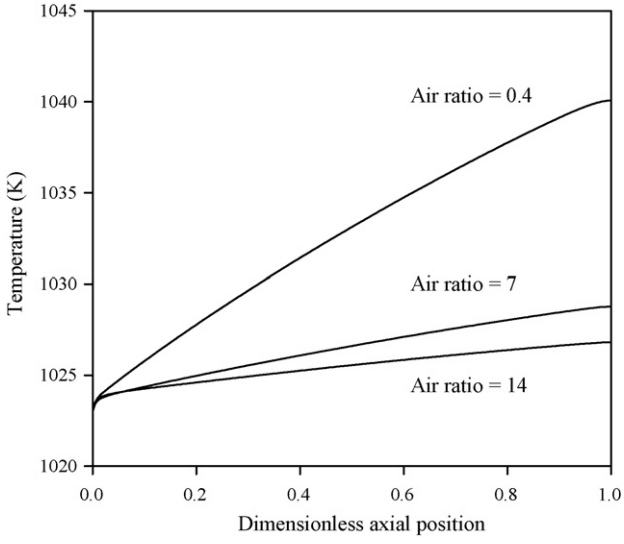

Fig. 5. Cathode stream temperature along the stack for an average current density of 7000 A m^{-2}, an inlet temperature of 1023 K and air ratios of 0.4, 7 and 14.

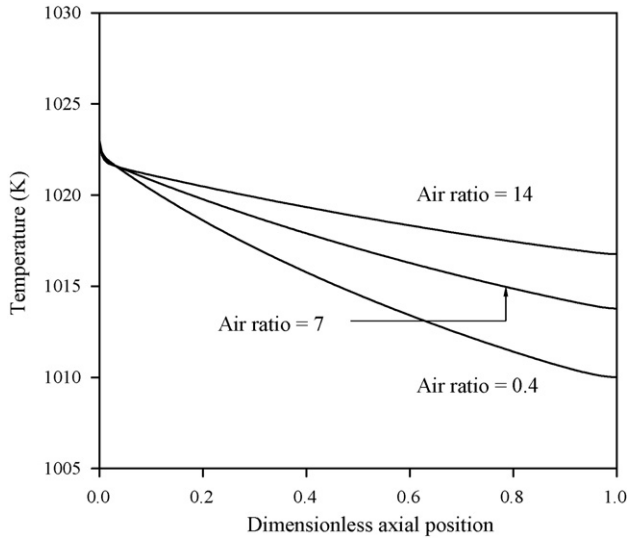

Fig. 6. Cathode stream temperature along the stack for an average current density of 5000 A m^{-2}, an inlet temperature of 1023 K and air ratios of 0.4, 7 and 14.

average current density may be compensated by an increased air ratio.

In spite of such a concept for the temperature control, closer observation of Figs. 5 and 6 reveals that, even at the outlet, the stack temperature only varies over the entire range of air ratios studied by around 13 K for the exothermic operation, and less than 7 K for the endothermic operation. Here, the weak dependence of the stack temperature on the air ratio is explained by the fact that the sets of operating conditions used in producing these results are close to thermoneutral operation. As illustrated later in this section, if a stack is instead operated at highly exothermic or endothermic conditions, the magnitude of the temperature gradient would be large along the stack and considerable temperature difference would exist between the inlet air and rest of the stack. Under such conditions, a significant transfer of heat between the cell components and air flow would occur, and the regulation of such a heat transfer, by the changes in the air flow rate, should result in a satisfactory temperature control. On the other hand, if a stack is operated close to the thermoneutral point, the magnitude of the temperature gradient would be small and the temperature of the inlet air flow would be similar to that of the rest of the stack. As a consequence, only a modest transfer of heat between the cell components and air flow would occur. The regulation of such a minor heat transfer, by the changes in the air flow rate, is not expected to create a significant influence over the stack temperature. Therefore the air ratio manipulation is not considered to provide a satisfactory temperature control for the conditions presented in Figs. 5 and 6.

Furthermore, if a stack is operated close to the thermoneutral point, there is an increased risk of encountering the transition between exothermic and endothermic operation even with the aid of the control strategy. For the conditions presented in Figs. 5 and 6, the decrease in the average current density from 7000 to 5000 A m^{-2} would result in the stack to switch from exothermic to endothermic mode. The selection of the operating conditions such that the stack is driven in more exothermic or endothermic conditions would prevent such transitions, avoiding the necessary changes in the system configurations.

In addition to the convective transfer of heat, the changes in the air flow has another effect on the stack temperature through the changes in O_2 partial pressure. The thermodynamics indicate that, assuming ideal gas behaviour of H_2, H_2O and O_2, the enthalpy change involved during the electrolysis reaction is independent of the partial pressure of the gases [35]. This implies that the total energy consumed by the reaction, per mole of product H_2, is not altered by the fall in the O_2 partial pressure caused by the dilution of the anode streams by the air flow. In contrast, the electrical energy consumed by the reaction, per mole of product H_2, is decreased by the fall in the O_2 partial pressure. This is evident in the previous sections where the introduction of the air flow to the anode channels caused the reduction in the reversible potential which is directly proportional to the electrical energy consumed by the reaction. During electrolysis, such a decrease in the electrical energy consumption is compensated by an increase in the thermal energy consumption, estimated in Fig. 7 as a function of air ratio. The figure has been produced using only the electrochemical model, without mass and energy balances, predicting the stack behaviour at one location along the stack, which is assumed to be at 1023 K here. The cathode stream composition, averaged over the stack length, is taken as 46 mol% H_2/54 mol% H_2O. The average anode stream compositions are determined for each air ratio values. In the figure, the thermal energy consumed increases from around 66.9 to 68.6 kJ mol^{-1} H_2 between the air ratios of 0.4 and 4 while a significantly smaller rise is observed above the air ratio of 4. This is because the reduction in the O_2 partial pressure involved when the air ratio is increased, for example, from 1 to 2 is considerably larger than that involved when the air ratio is increased from 7 to 8. During exothermic operation, the increase in the thermal energy consumption, associated with the rise in the air

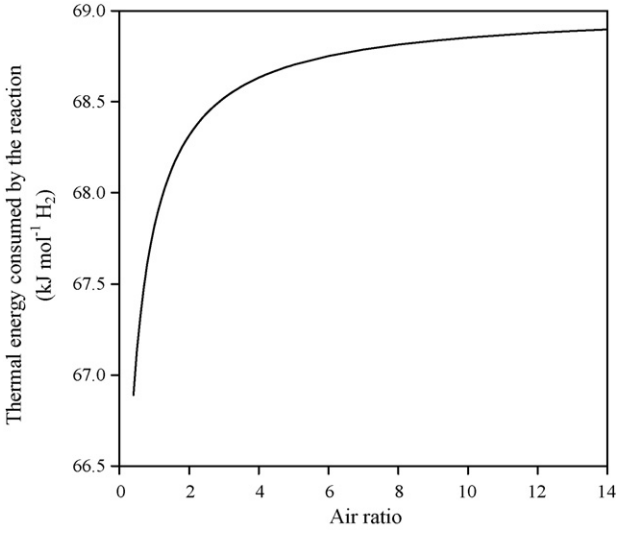

Fig. 7. Thermal energy consumed by the reaction, per mole of product H_2, as a function of the air ratio at 1023 K. The cathode stream compositions are taken as 46 mol% H_2/54 mol% H_2O.

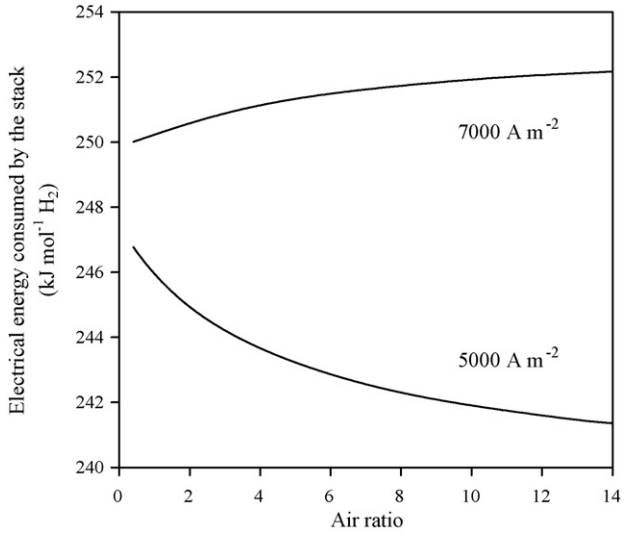

Fig. 8. Electrical energy consumed by the stack, per mole of product H_2, as a function of the air ratio, for average current densities of 7000 and 5000 A m^{-2}, and an inlet temperature of 1023 K.

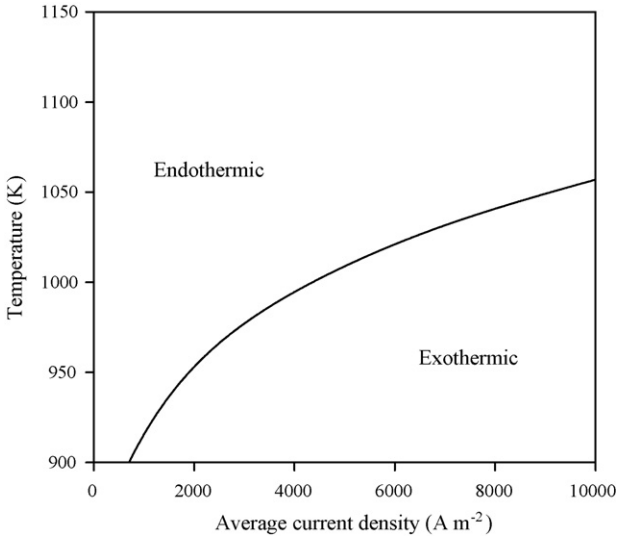

Fig. 9. Cathode and anode stream inlet temperature corresponding to the thermoneutral stack operation as a function of the average current density. The air ratio is fixed at 7.

ratio, complements the enhanced convective cooling supplied by the increased air flow. During endothermic operation, on the other hand, the increased thermal energy consumption competes against the enhanced convective heating. This is consistent with the exothermic and endothermic stack temperature distributions presented in Figs. 5 and 6, respectively, in which a greater change in the stack temperature is observed for the exothermic stack than for the endothermic stack between the air ratio of 0.4 and 7.

Fig. 8 presents the electrical energy consumed by exothermic and endothermic stack operation at average current densities of 7000 and 5000 A m^{-2}, respectively, as a function of the air ratio. From the previous discussion, the electrical energy consumed by the reaction at a given temperature is expected to decrease with an increasing air ratio. However, the electrical energy consumed across the stack, here operating in exothermic mode, is predicted to increase. This is due to the increase in the irreversible losses, associated with the decreased stack temperature, which prevails over the decrease in the reversible potential. For the endothermic stack, on the other hand, both the reversible potential and irreversible losses decrease with an increasing air ratio. The overall reduction in the electrical energy consumption of the endothermic stack, shown in the figure, indicates that the electrical efficiency of the stack is improved at higher air ratios. During the selection of the operating conditions, however, such advantages accruing from the increased air ratio must be offset against the significant extra energy required to generate the increased air flow rate.

As previously mentioned, SOEC stacks are not expected to maintain an effective temperature control when operated near thermoneutral conditions. The cathode and anode stream inlet temperature for which the stack operates in the thermoneutral mode is presented in Fig. 9, as a function of the average current density. The figure is produced by introducing to the model an additional constraint by which the sum of all the enthalpy changes involved in the electrolysis reaction along the stack is matched by the electrical energy consumed by the stack. That is to say that the supplied electrical power not only provides the electrical energy necessary for the electrolysis but also allows the generation, through the irreversible losses, of the precise quantity of the thermal energy required for the reaction. Note that the curve in Fig. 9 represents the stack operation where thermoneutral conditions are met at every location along the stack and not the situation in which the thermoneutral conditions are only satisfied at the inlet by the local values of the current density, temperature and stream compositions. Furthermore, as both the thermal energy consumed by the electrolysis reaction and the heat produced by the irreversible losses depend on the stream compositions, the thermoneutral conditions predicted here for the IT-SOEC stack with air-fed anode channels would be different to those expected for the IT-SOEC stack with pure O_2 anode streams.

The regions below and above the curve in Fig. 9 correspond to the conditions for exothermic and endothermic operations, respectively. For average current densities of 7000 and 5000 A m^{-2}, an inlet temperature of 1023 K results in the stack operating near the thermoneutral point. However, by adjusting the inlet temperature for the 7000 A m^{-2} case to 923 K and that for the 5000 A m^{-2} case to 1123 K, the stack can be driven at more exothermic or endothermic conditions, respectively. The cathode stream temperature distributions along such exothermic and endothermic stacks are presented in Figs. 10 and 11, respectively. The shift away from the thermoneutral point is evident in both figures with an increased temperature difference between the inlet and outlet. For an air ratio of 7, such a temperature difference is as large as 88 K during exothermic operation and 63 K during endothermic operation. The consequent increase in the influence of the air ratio on the stack temperature is also observed, with the outlet temperature ranging by more than 120 and 90 K in Figs. 10 and 11, respectively. The manipulation of the air ratio is considered to provide an effective means of temperature control under these condi-

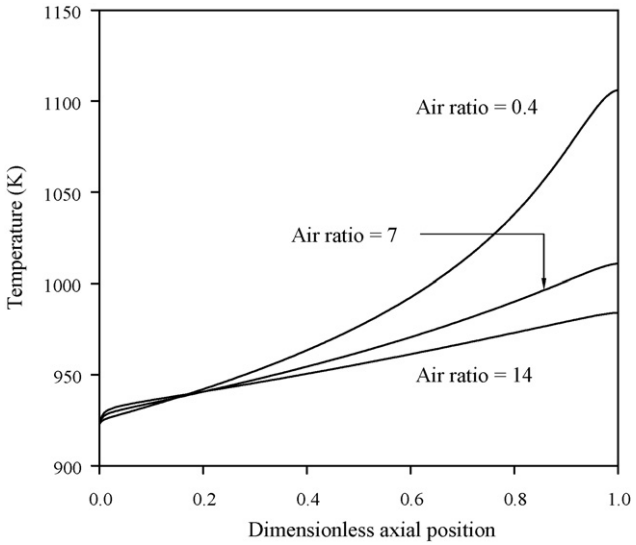

Fig. 10. Cathode stream temperature along the stack for an average current density of 7000 A m^{-2}, an inlet temperature of 923 K and air ratios of 0.4, 7 and 14.

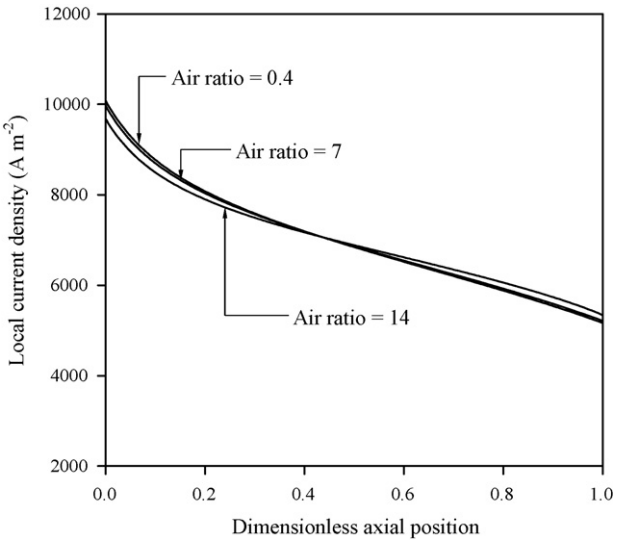

Fig. 12. Local current density along the stack for an average current density of 7000 A m^{-2}, an inlet temperature of 1023 K and air ratios of 0.4, 7 and 14.

tions. The dynamic response of the exothermic and endothermic stacks operated under these conditions will be presented in a subsequent publication.

3.3. Relationship between the stack temperature and current density

Figs. 12 and 13 show the local current density distributions for the IT-SOEC stack with air-fed anode channels operated at average current densities of 7000 and 5000 A m^{-2}, respectively. The air ratio is varied between 0.4 and 14 while the inlet temperature is maintained at 1023 K. In both figures, the curve displays little dependence on the air ratio and decreases in value towards the outlet. Generally along an SOEC stack, low local current densities are observed where increased voltage requirements exist. Those are the locations with higher H_2 and O_2 partial pressure, lower H_2O partial pressure, and reduced temperature. Therefore, as H_2 and O_2 are generated and H_2O is consumed along the stack, the resulting change in the stream compositions tends to decrease the local current density towards the outlet. Furthermore, the positive temperature gradient along an exothermic stack, and the negative temperature gradient along an endothermic stack, respectively act to increase and decrease the local current density towards the outlet. During exothermic operation, the effects of the changing stream compositions and the positive temperature gradient compete against one another. Here, the decrease in the local current density along the stack in Fig. 12 indicates that the effect of the changing stream com-

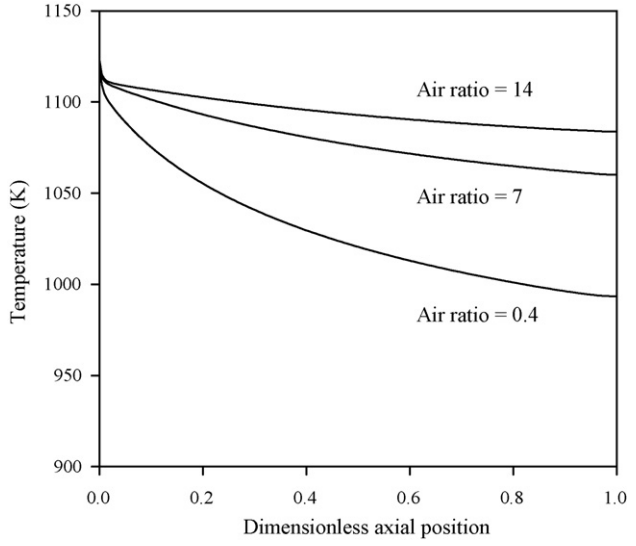

Fig. 11. Cathode stream temperature along the stack for an average current density of 5000 A m^{-2}, an inlet temperature of 1123 K and air ratios of 0.4, 7 and 14.

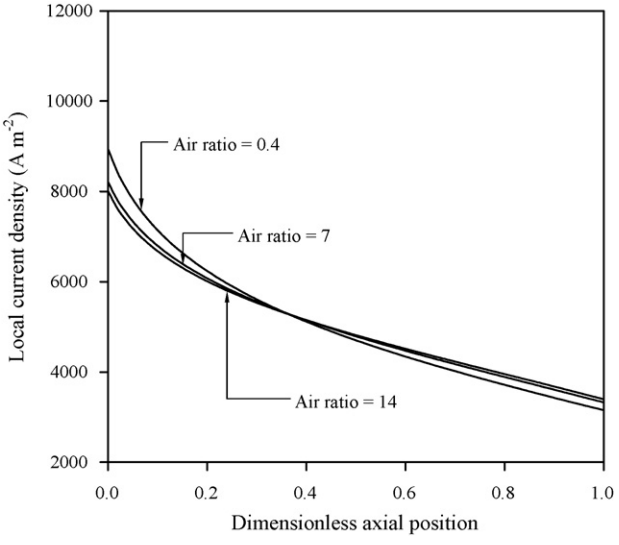

Fig. 13. Local current density along the stack for an average current density of 5000 A m^{-2}, an inlet temperature of 1023 K and air ratios of 0.4, 7 and 14.

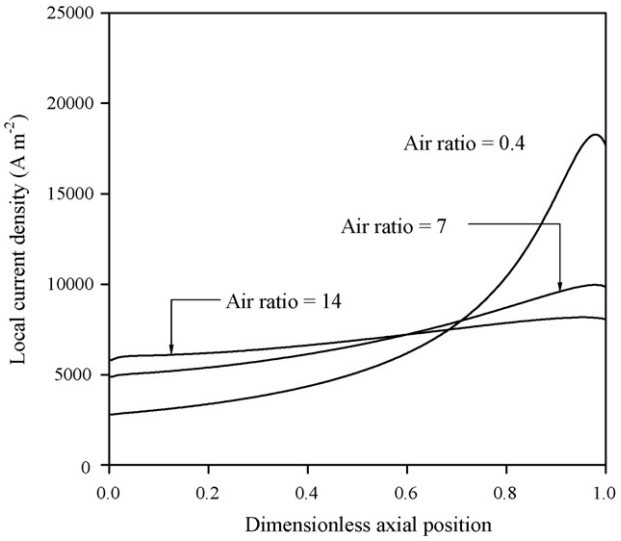

Fig. 14. Local current density along the stack for an average current density of 7000 A m^{-2}, an inlet temperature of 923 K and air ratios of 0.4, 7 and 14.

positions prevails. This is consistent with the small temperature gradient observed in Fig. 5, which is not expected to significantly influence the local current density distributions. For endothermic operation in Fig. 13, the changes in stream compositions and the negative temperature gradient both contribute to decreasing the local current density along the stack.

The local current density distribution for the IT-SOEC stack with air-fed anode channels operated at an average current density of 7000 A m^{-2} and an inlet stream temperature of 923 K is presented in Fig. 14, and that for the IT-SOEC stack with air-fed anode channels operated at an average current density of 5000 A m^{-2} and an inlet stream temperature of 1123 K is illustrated in Fig. 15. In Fig. 14, the increase in the local current density along the exothermic stack indicates that the effect of the changing stream compositions is overwhelmed by the effect of the temperature gradient. Here, the local current density distribution is significantly influenced by the large temperature gradient shown in Fig. 10. For the endothermic stack, the changing stream compositions and negative temperature gradient again both contribute to a decrease in the local current density towards the outlet as shown in Fig. 15. The increased dependence of the local current density distribution on the air ratio in Figs. 14 and 15 is a consequence of the enhanced impact of the air ratio on the stack temperature gradient, evident in Figs. 10 and 11.

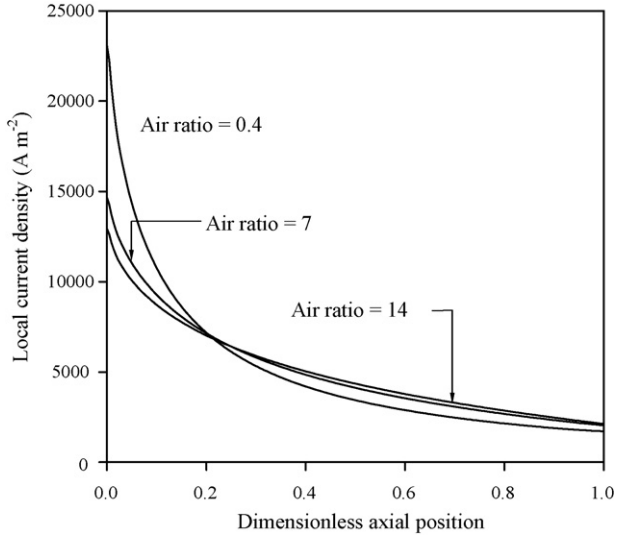

Fig. 15. Local current density along the stack for an average current density of 5000 A m^{-2}, an inlet temperature of 1123 K and air ratios of 0.4, 7 and 14.

As the current density is directly related to the reaction rate through Faraday's law, assuming a current efficiency of 100%, the positive local current density gradient in Fig. 14 corresponds to an increase in the H_2 generation rate along the stack. During exothermic operation, such an accelerated reaction acts to increase the rate of the temperature rise towards the outlet. Although there are other factors which influence the temperature distribution along the stack, this increase in the reaction rate contributes to creating the temperature distribution to concave upwards in Fig. 10. Such an effect is more pronounced for operation with a low air ratio where the stack temperature is not dominated by the convective heat transfer between the cell components and air flow. For endothermic operation, on the other hand, the negative local current density gradient in Fig. 15 and the associated reduction in the reaction rate along the stack tend to decrease the rate of the temperature fall towards the outlet. Such an effect is observed in Fig. 11 as the stack temperature distributions, which also concave upwards.

4. Conclusions

A one-dimensional distributed dynamic model of a cathode-supported planar IT-SOEC stack with the air flow introduced through the cells has been presented. The model has been employed to study the steady state behaviour of such an SOEC and the prospect for stack temperature control through variation of the air flow rate. Steady state performance analysis has shown that the dilution of the product O_2 by the air on the anode side of the cells causes a reduction in the reversible cell potential. Activation overpotentials were predicted to provide the largest contribution to the irreversible losses while concentration overpotentials remained insignificant throughout, in spite of the electrode-supported nature of the cells. Evaluation of the control strategy showed that an increase in the air flow rate provides enhanced cooling and heating during the exothermic and endothermic stack operation respectively, prompting the temperature to become more uniformly distributed along the stack. However, only a small dependence of the temperature on the air flow rate was observed for a stack driven at conditions near thermoneutral operation, indicating that this operating mode should be avoided from a control perspective. To further analyse the control strategy, the dynamic response of the stack will be presented in the future.

References

[1] D.L. Stojic, M.P. Marceta, S.P. Sovilj, S.S. Miljanic, J. Power Sources 118 (2003) 315–319.
[2] S. Dutta, Int. J. Hydrogen Energy 15 (1990) 379–386.

[3] T. Kobayashi, K. Abe, Y. Ukyo, H. Matsumoto, Solid State Ionics 138 (2001) 243–251.
[4] T. Schober, Solid State Ionics 139 (2001) 95–104.
[5] H. Matsumoto, M. Okubo, S. Hamajima, K. Katahira, H. Iwahara, Solid State Ionics 152/153 (2002) 715–720.
[6] P. Aguiar, C.S. Adjiman, N.P. Brandon, J. Power Sources 138 (2004) 120–136.
[7] J.S. Herring, J.E. O'Brien, C.M. Stoots, G.L. Hawkes, J.J. Hartvigsen, M. Shahnam, Int. J. Hydrogen Energy 32 (2007) 440–450.
[8] W. Donitz, E. Erdle, Int. J. Hydrogen Energy 10 (1985) 291–295.
[9] R. Hino, K. Haga, H. Aita, K. Sekita, Nucl. Eng. Des. 233 (2004) 363–375.
[10] W. Doenitz, R. Schmidberger, Int. J. Hydrogen Energy 7 (1982) 321–330.
[11] J.S. Herring, P. Lessing, J.E. O'Brien, C. Stoots, J. Hartvigsen, S. Elangovan, Proceedings of the 2nd Information Exchange Meeting on Nuclear Production of Hydrogen, 2003, pp. 183–200.
[12] J. Larminie, A. Dicks, Fuel Cell Systems Explained, 2nd ed., Wiley, 2003.
[13] J. Udagawa, P. Aguiar, N.P. Brandon, J. Power Sources 166 (2007) 127–136.
[14] K.H. Quandt, R. Streicher, Int. J. Hydrogen Energy 11 (1986) 309–315.
[15] P. Aguiar, C.S. Adjiman, N.P. Brandon, J. Power Sources 147 (2005) 136–147.
[16] G.Y. Lai, High-temperature Corrosion of Engineering Alloys, ASM International, 1990.
[17] B. Yildiz, M.S. Kazimi, Int. J. Hydrogen Energy 31 (2006) 77–92.
[18] F. Werkoff, J. Sigurvinsson, C. Mansilla, P. Lovera, Proceedings of the 16th World Hydrogen Energy Conference, 2006 (CD-ROM).
[19] J. Sigurvinsson, C. Mansilla, P. Lovera, F. Werkoff, Int. J. Hydrogen Energy 32 (2007) 1174–1182.
[20] J. Sigurvinsson, C. Mansilla, B. Arnason, A. Bontemps, A. Marechal, T.I. Sigfusson, F. Werkoff, Energy Convers. Manage. 47 (2006) 3543–3551.
[21] Y. Shin, W. Park, J. Chang, J. Park, Int. J. Hydrogen Energy 32 (2007) 1486–1491.
[22] M. Saxe, P. Alvfors, Energy 32 (2007) 42–50.
[23] J.W. Park, Y.J. Lee, Proceedings of the 2006 International Congress on Advances in Nuclear Power Plants, 2006 (CD-ROM).
[24] C. Mansilla, J. Sigurvinsson, A. Bontemps, A. Marechal, F. Werkoff, Energy 32 (2007) 423–430.
[25] M. Ni, M.K.H. Leung, D.Y.C. Leung, Electrochim. Acta 52 (2007) 6707–6718.
[26] M. Ni, M.K.H. Leung, D.Y.C. Leung, Int. J. Hydrogen Energy 32 (2007) 2305–2313.
[27] P. Lovera, F. Blein, J. Vulliet, Proceedings of the 16th World Hydrogen Energy Conference, 2006 (CD-ROM).
[28] E. Hoashi, T. Ogawa, K. Matsunaga, K. Nakada, S. Fujiwara, S. Kasai, Proceedings of the 2006 International Congress on Advances in Nuclear Power Plants, 2006 (CD-ROM).
[29] G.L. Hawkes, J.E. O'Brien, C.M. Stoots, J.S. Herring, M. Shahnam, Nucl. Technol. 158 (2007) 132–144.
[30] G. Hawkes, J. O'Brien, C. Stoots, J. Herring, R. Jones, Proceedings of the 2006 Fuel Cell Seminar, 2006 (CD-ROM).
[31] P. Iora, P. Aguiar, C.S. Adjiman, N.P. Brandon, Chem. Eng. Sci. 60 (2005) 2963–2975.
[32] S.H. Chan, K.A. Khor, Z.T. Xia, J. Power Sources 93 (2001) 130–140.
[33] J. Kim, A.V. Virkar, K. Fung, K. Mehta, S.C. Singhal, J. Electrochem. Soc. 146 (1999) 69–78.
[34] Process Systems Enterprise Ltd., gPROMS Introductory User Guide, 2002.
[35] M.J. Moran, H.N. Shapiro, Fundamentals of Engineering Thermodynamics, 4th ed., John Wiley & Sons, 2000.